Supplemental Materials

Lattice interactions

For our LO lattice calculations we use a spatial lattice spacing $a = (100\ \text{MeV})^{-1} = 1.97$ fm and time lattice step $a_t = (150\ \text{MeV})^{-1} = 1.32$ fm. Our axial-vector coupling constant is $g_A = 1.29$ as derived from the Goldberger-Treiman relation, the pion decay constant is $f_\pi = 92.2$ MeV, and the pion mass is $M_\pi = M_{\pi^0} = 134.98$ MeV. For the nucleon mass we use $m = 938.92$ MeV, and the electromagnetic fine structure constant is $\alpha_{\text{EM}} = (137.04)^{-1}$. We don't consider any isospin-breaking terms other than the Coulomb interaction in these LO calculations. We use σ_S with $S = 1, 2, 3$ for the Pauli matrices acting upon spin, and τ_I with $I = 1, 2, 3$ for the Pauli matrices acting upon isospin. We will use lattice units where the quantities are multiplied by the appropriate power of the spatial lattice spacing a to make the combination dimensionless. We write α_t for the ratio a_t/a. We use the notation $\sum_{\langle \mathbf{n}'\,\mathbf{n}\rangle}$ to denote the summation over nearest-neighbor lattice sites of $\mathbf{n}$. We write $\sum_{\langle \mathbf{n}'\,\mathbf{n}\rangle_i}$ to indicate the sum over nearest-neighbor lattice sites of $\mathbf{n}$ along the i^{th} spatial axis. Similarly, we define $\sum_{\langle\langle \mathbf{n}'\,\mathbf{n}\rangle\rangle_i}$ as the sum over next-to-nearest-neighbor lattice sites of $\mathbf{n}$ along the i^{th} axis and $\sum_{\langle\langle\langle \mathbf{n}'\,\mathbf{n}\rangle\rangle\rangle_i}$ as the sum over next-to-next-to-nearest-neighbor lattice sites of $\mathbf{n}$ along the i^{th} axis. Our lattice geometry is chosen to be an L^3 periodic lattice, and so the summations over $\mathbf{n}'$ are defined using periodic boundary conditions.

For each lattice site $\mathbf{n}$ on our lattice and real parameter s_{NL}, we define nonlocal annihilation and creation operators for each spin and isospin component of the nucleon,

$$a_{\text{NL}}(\mathbf{n}) = a(\mathbf{n}) + s_{\text{NL}} \sum_{\langle \mathbf{n}'\,\mathbf{n}\rangle} a(\mathbf{n}'), \tag{1}$$

$$a^\dagger_{\text{NL}}(\mathbf{n}) = a^\dagger(\mathbf{n}) + s_{\text{NL}} \sum_{\langle \mathbf{n}'\,\mathbf{n}\rangle} a^\dagger(\mathbf{n}'). \tag{2}$$

For spin indices $S = 1, 2, 3$, and isospin indices $I = 1, 2, 3$, we define point-like densities,

$$\rho(\mathbf{n}) = a^\dagger(\mathbf{n})a(\mathbf{n}), \tag{3}$$

$$\rho_S(\mathbf{n}) = a^\dagger(\mathbf{n})[\sigma_S]a(\mathbf{n}), \tag{4}$$

$$\rho_I(\mathbf{n}) = a^\dagger(\mathbf{n})[\tau_I]a(\mathbf{n}), \tag{5}$$

$$\rho_{S,I}(\mathbf{n}) = a^\dagger(\mathbf{n})[\sigma_S \otimes \tau_I]a(\mathbf{n}). \tag{6}$$

For spin indices $S = 1, 2, 3$, and isospin indices $I = 1, 2, 3$, we also define smeared nonlocal densities,

$$\rho_{\text{NL}}(\mathbf{n}) = a^\dagger_{\text{NL}}(\mathbf{n})a_{\text{NL}}(\mathbf{n}), \tag{7}$$

$$\rho_{S,\text{NL}}(\mathbf{n}) = a^\dagger_{\text{NL}}(\mathbf{n})[\sigma_S]a_{\text{NL}}(\mathbf{n}), \tag{8}$$

$$\rho_{I,\text{NL}}(\mathbf{n}) = a^\dagger_{\text{NL}}(\mathbf{n})[\tau_I]a_{\text{NL}}(\mathbf{n}), \tag{9}$$

$$\rho_{S,I,\text{NL}}(\mathbf{n}) = a^\dagger_{\text{NL}}(\mathbf{n})[\sigma_S \otimes \tau_I]a_{\text{NL}}(\mathbf{n}), \tag{10}$$

and smeared local densities for real parameter s_{L},

$$\rho_{\text{L}}(\mathbf{n}) = a^\dagger(\mathbf{n})a(\mathbf{n}) + s_{\text{L}} \sum_{\langle \mathbf{n}'\,\mathbf{n}\rangle} a^\dagger(\mathbf{n}')a(\mathbf{n}'), \tag{11}$$

$$\rho_{S,\text{L}}(\mathbf{n}) = a^\dagger(\mathbf{n})[\sigma_S]a(\mathbf{n}) + s_{\text{L}} \sum_{\langle \mathbf{n}'\,\mathbf{n}\rangle} a^\dagger(\mathbf{n}')[\sigma_S]a(\mathbf{n}'), \tag{12}$$

$$\rho_{I,\text{L}}(\mathbf{n}) = a^\dagger(\mathbf{n})[\tau_I]a(\mathbf{n}) + s_{\text{L}} \sum_{\langle \mathbf{n}'\,\mathbf{n}\rangle} a^\dagger(\mathbf{n}')[\tau_I]a(\mathbf{n}'), \tag{13}$$

$$\rho_{S,I,\text{L}}(\mathbf{n}) = a^\dagger(\mathbf{n})[\sigma_S \otimes \tau_I]a(\mathbf{n}) + s_{\text{L}} \sum_{\langle \mathbf{n}'\,\mathbf{n}\rangle} a^\dagger(\mathbf{n}')[\sigma_S \otimes \tau_I]a(\mathbf{n}'). \tag{14}$$

The nonlocal short-range interactions are written as

$$V_{\text{NL}} = \frac{c_{\text{NL}}}{2} \sum_{\mathbf{n}} :\rho_{\text{NL}}(\mathbf{n})\rho_{\text{NL}}(\mathbf{n}): + \frac{c_{I,\text{NL}}}{2} \sum_{\mathbf{n},I} :\rho_{I,\text{NL}}(\mathbf{n})\rho_{I,\text{NL}}(\mathbf{n}):, \tag{15}$$

while the local short-range interactions are

$$V_{\rm L} = \frac{c_{\rm L}}{2}\sum_{\mathbf{n}} :\rho_{\rm L}(\mathbf{n})\rho_{\rm L}(\mathbf{n}): + \frac{c_{S,{\rm L}}}{2}\sum_{\mathbf{n},S} :\rho_{S,{\rm L}}(\mathbf{n})\rho_{S,{\rm L}}(\mathbf{n}): + \frac{c_{I,{\rm L}}}{2}\sum_{\mathbf{n},I} :\rho_{I,{\rm L}}(\mathbf{n})\rho_{I,{\rm L}}(\mathbf{n}): + \frac{c_{S,I,{\rm L}}}{2}\sum_{\mathbf{n},S,I} :\rho_{S,I,{\rm L}}(\mathbf{n})\rho_{S,I,{\rm L}}(\mathbf{n}): . \tag{16}$$

The :: symbol indicates normal ordering, where the annihilation operators are on the right-hand side and the creation operators are on the left-hand side. As described in previous work [1], we take special combinations of the four local short-range operator coefficients so that the interaction in odd partial waves vanish completely. For our work here, we also make the strength of the local short-range interactions equal in the two S-wave channels. As a result, we have only one independent coefficient, $c_{S,{\rm L}} = c_{I,{\rm L}} = c_{S,I,{\rm L}} = -\frac{1}{3}c_{\rm L}$. In future work it may be useful to consider relaxing this condition.

The one-pion exchange interaction has the form

$$V_{\rm OPE} = -\frac{g_A^2}{8f_\pi^2}\sum_{\mathbf{n}',\mathbf{n},S',S,I} :\rho_{S',I}(\mathbf{n}')f_{S'S}(\mathbf{n}'-\mathbf{n})\rho_{S,I}(\mathbf{n}):, \tag{17}$$

where $f_{S'S}$ is defined as

$$f_{S'S}(\mathbf{n}'-\mathbf{n}) = \frac{1}{L^3}\sum_{\mathbf{q}}\frac{\exp[-i\mathbf{q}\cdot(\mathbf{n}'-\mathbf{n}) - b_\pi\mathbf{q}^2]q_{S'}q_S}{\mathbf{q}^2+M_\pi^2}, \tag{18}$$

and each lattice momentum component q_S is an integer multiplied by $2\pi/L$. The parameter b_π is included to remove short-distance lattice artifacts in the one-pion exchange interaction. It results in better preservation of rotational symmetry and will be especially useful at smaller lattice spacings [2]. The Coulomb interaction can be written as

$$V_{\rm Coulomb} = -\frac{\alpha_{\rm EM}}{2}\sum_{\mathbf{n}',\mathbf{n}} :\frac{1}{4}[\rho(\mathbf{n}')+\rho_{I=3}(\mathbf{n}')]\frac{1}{d(\mathbf{n}'-\mathbf{n})}[\rho(\mathbf{n})+\rho_{I=3}(\mathbf{n})]:, \tag{19}$$

where $d(\mathbf{n}'-\mathbf{n})$ is the shortest length of $\mathbf{n}'-\mathbf{n}$ as measured on the periodic lattice, and we define the value of d at the origin to be $\frac{1}{2}$. Our notation $\rho_{I=3}$ refers to the $I=3$ isospin component of ρ_I. We use a free lattice Hamiltonian [1] of the form,

$$H_{\rm free} = \frac{49}{12m}\sum_{\mathbf{n}}a^\dagger(\mathbf{n})a(\mathbf{n}) - \frac{3}{4m}\sum_{\mathbf{n},i}\sum_{\langle\mathbf{n}'\,\mathbf{n}\rangle_i}a^\dagger(\mathbf{n}')a(\mathbf{n}) + \frac{3}{40m}\sum_{\mathbf{n},i}\sum_{\langle\langle\mathbf{n}'\,\mathbf{n}\rangle\rangle_i}a^\dagger(\mathbf{n}')a(\mathbf{n}) - \frac{1}{180m}\sum_{\mathbf{n},i}\sum_{\langle\langle\langle\mathbf{n}'\,\mathbf{n}\rangle\rangle\rangle_i}a^\dagger(\mathbf{n}')a(\mathbf{n}). \tag{20}$$

For interaction A at LO, the lattice Hamiltonian is

$$H_{\rm A} = H_{\rm free} + V_{\rm NL} + V_{\rm OPE}, \tag{21}$$

with $s_{\rm NL} = 0.07700$, $c_{\rm NL} = -0.2268$, $c_{I,{\rm NL}} = 0.02184$, and $b_\pi = 0.7000$. These parameters are determined by fitting to the low-energy nucleon-nucleon phase shifts and the observed deuteron energy. For the corresponding LO + Coulomb interactions, we simply add $V_{\rm Coulomb}$ to $H_{\rm A}$.

For interaction B at LO, we have

$$H_{\rm B} = H_{\rm free} + V_{\rm NL} + V_{\rm L} + V_{\rm OPE}, \tag{22}$$

with $s_{\rm NL} = 0.07700$, $s_{\rm L} = 0.8100$, $c_{\rm NL} = -0.1171$, $c_{I,{\rm NL}} = 0.02607$, $c_{\rm L} = -0.01013$, and $b_\pi = 0.7000$. For the corresponding LO + Coulomb interactions, we simply add $V_{\rm Coulomb}$ to $H_{\rm B}$. These parameters are determined by fitting to the low-energy nucleon-nucleon phase shifts, the observed deuteron energy, and the low-energy alpha-alpha S-wave phase shifts.

We should clarify that the ^{4}He energy is not used to fit the parameters of interactions A and B. However we do observe a strong correlation between the alpha-alpha S-wave phase shifts and the shape of the ^{4}He wave function tail. This has the resulting effect of driving the ^{4}He energy close to the physical value when we tune the parameters of interaction B to the alpha-alpha S-wave phase shifts. The parameters of interaction A are determined by starting from the parameters of interaction B, setting the local short-range interactions to zero, and then tuning the coefficients of the nonlocal short-range interactions to the nucleon-nucleon phase shifts and deuteron energy.

Nucleon-nucleon scattering

We use the spherical wall method to calculate lattice phase shifts [3, 4]. We use the improvements recently introduced in Ref. [5]. Let $|\mathbf{n}\rangle \otimes |S_z\rangle$ be the two-nucleon scattering state with lattice separation vector $\mathbf{n}$ and z-component of total intrinsic spin S_z. We define radial coordinates on the lattice by grouping together lattice mesh points with the same radial distance to define radial position states and project onto states with total angular momentum J, J_z in the continuum limit. Using spherical harmonics Y_{ℓ,ℓ_z} with orbital angular momentum ℓ, ℓ_z and Clebsch-Gordan coefficients $C^{J,J_z}_{\ell,\ell_z,S,S_z}$, we define

$$|r\rangle_L^{J,J_z} = \sum_{\mathbf{n},\ell_z,S_z} C^{J,J_z}_{\ell,\ell_z,S,S_z} Y_{\ell,\ell_z}(\hat{\mathbf{n}}) \delta_{r,|\mathbf{n}|} |\mathbf{n}\rangle \otimes |S_z\rangle, \tag{23}$$

where $\delta_{r,|\mathbf{n}|}$ is a Kronecker delta function that selects lattice points where $|\mathbf{n}| = r$. This angular momentum projection allows us to calculate partial-wave phase shifts on the lattice as in Ref. [5].

As described in Ref. [5], we impose a hard spherical wall boundary at some large radius R_W and a smooth auxiliary Gaussian potential in front of the wall, which we call $V_{\rm aux}(r)$. For our calculations here we use $R_W = 15.02$ lattice units. The auxiliary potential has the form

$$V_{\rm aux}(r) = V_0 \exp\left[-(r - R_W)^2\right], \tag{24}$$

with adjustable coefficient V_0 that is used to probe different values of the scattering energy. The auxiliary potential is non-negligible only when r is a few lattice units away the wall at R_W. We determine the asymptotic phase shifts from the radial wave function at points where r is large but $V_{\rm aux}(r)$ is negligible. For coupled partial waves such as the ${}^3s_1 - {}^3d_1$ channel, we determine the two phase shifts and mixing angle using an additional auxiliary potential $U_{\rm aux}(r)$ with the same functional form as $V_{\rm aux}(r)$, but with imaginary Hermitian off-diagonal couplings between the two partial waves,

$$\begin{bmatrix} 0 & iU_{\rm aux}(r) \\ -iU_{\rm aux}(r) & 0 \end{bmatrix}. \tag{25}$$

This complex-valued auxiliary potential breaks time-reversal invariance and allows us to extract information about the two independent phase shifts and mixing angle from the real and imaginary parts of the complex-valued wave functions.

In Fig. S1 we show LO lattice phase shifts for proton-neutron scattering versus the center-of-mass relative momentum for interactions A (red triangles) and B (blue squares). For comparison we also plot the phase shifts extracted from the Nijmegen partial wave analysis [6] (black lines) and a continuum version of interaction A (green dashed lines). In the first row, the data in panels **a**, **b**, **c**, **d** correspond to ${}^1S_0, {}^3S_1, {}^1P_1, {}^3P_0$ respectively. In the second row, panels **e**, **f**, **g**, **h** correspond to ${}^3P_1, {}^3P_2, {}^1D_2, {}^3D_1$ respectively. In the third row, panels **i**, **j**, **k**, **l** correspond to ${}^3D_2, {}^3D_3, \varepsilon_1, \varepsilon_2$ respectively. The level of agreement with the experimental phase shifts for interactions A and B is typical for LO chiral effective field theory at our cutoff momentum of $\pi/a \approx 314$ MeV. The agreement would be somewhat better if we were to use a smaller value of the smearing parameter b_π in the one-pion exchange potential. However, we prefer the higher value of b_π to reduce sign oscillations in the Monte Carlo lattice simulations. The LO interactions are more than sufficient to illustrate the ideas of this work but not sufficient for precision calculations. For precision calculations, this would be just the first step in the chiral effective field theory expansion, and the phase shifts would be systematically improved at each higher order, NLO, NNLO, and so on.

We note the good agreement between the continuum results in green dashed lines and lattice interaction A results. This is a good indication that we have successfully reduced lattice artifacts from the calculations and was part of the motivation for introducing the parameter b_π. The nonlocal smeared interaction $V_{\rm NL}$ makes a non-negligible contribution to the S-wave interactions only. Furthermore, the local smeared interaction $V_{\rm L}$ makes a nonzero contribution to only the even partial waves (S, D, $\cdots$). Hence the interactions A and B are exactly the same in all odd partial waves. We see that the S-wave interactions for interactions A and B are also quite similar, though the ${}^1S_0$ partial wave scattering is somewhat more attractive for interaction A. On the other hand, the D-wave partial waves are more attractive for interaction B.

FIG. S1: Nucleon-nucleon scattering phase shifts. We plot LO lattice phase shifts for proton-neutron scattering versus the center-of-mass relative momentum for interactions A (red triangles) and B (blue squares). For comparison we also plot the phase shifts extracted from the Nijmegen partial wave analysis [6] (black lines) and a continuum version of interaction A (green dashed lines). In the first row, the data in panels **a**, **b**, **c**, **d** correspond to ${}^1S_0, {}^3S_1, {}^1P_1, {}^3P_0$ respectively. In the second row, panels **e**, **f**, **g**, **h** correspond to ${}^3P_1, {}^3P_2, {}^1D_2, {}^3D_1$ respectively. In the third row, panels **i**, **j**, **k**, **l** correspond to ${}^3D_2, {}^3D_3, \varepsilon_1, \varepsilon_2$ respectively.

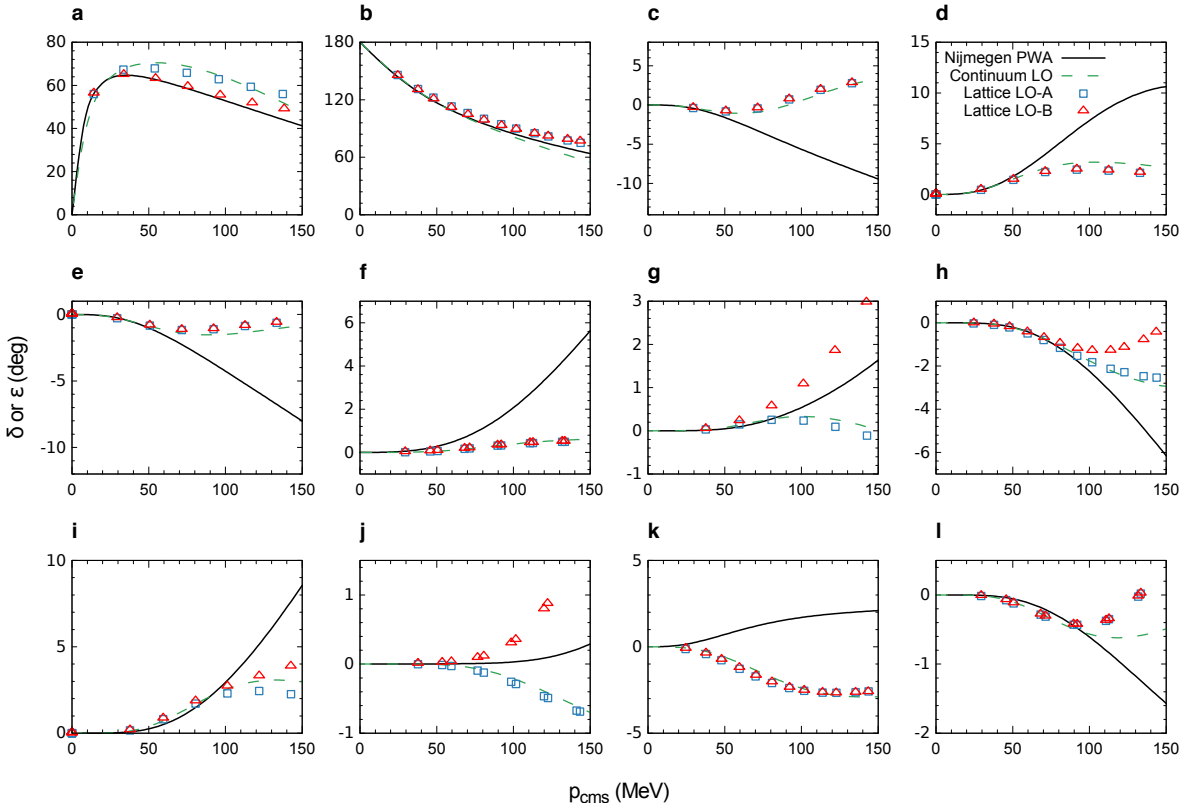

Euclidean time projection and auxiliary-field Monte Carlo

In these lattice simulations we work with the Euclidean time transfer matrix M, which is defined as the normal-ordered exponential of the lattice Hamiltonian H over one time lattice step,

$$M =: \exp[-H\alpha_t] : . \tag{26}$$

We consider some initial state $|\Psi_i\rangle$ and final state $|\Psi_f\rangle$ that have nonzero overlap with the ground state of interest. By applying successive powers of M upon $|\Psi_i\rangle$, the excited states decay away, and we can project out only the ground state. We calculate projection amplitudes of the form

$$A_{fi}(L_t) = \langle\Psi_f|M^{L_t}|\Psi_i\rangle. \tag{27}$$

By calculating the ratio $A_{fi}(L_t)/A_{fi}(L_t-1)$ for large L_t we can determine the ground state energy. In order to calculate first-order corrections to the ground state energy due to an additional term ΔH in the Hamiltonian, we also calculate the projection amplitude

$$A^{\Delta}_{fi}(L_t) = \langle\Psi_f|M^{\frac{L_t-1}{2}} M_\Delta M^{\frac{L_t-1}{2}}|\Psi_i\rangle, \tag{28}$$

for odd L_t, where

$$M_\Delta =: \exp[-(H+\Delta H)\alpha_t] : . \tag{29}$$

The corrections due to $H_{\rm Coulomb}$ are computed in this manner.

In most cases it is advantageous to first prepare the initial state using a simpler transfer matrix M_* which is an approximation to M. We choose M_* to be invariant under Wigner's SU(4) symmetry [7] where the four spin-isospin combinations of the nucleon transform into one another. The SU(4) symmetry eliminates sign oscillations from auxiliary-field Monte Carlo simulations of M_* [8, 9]. M_* has the same form as M, but the coefficients of operators that violate SU(4) symmetry are turned off. We use M_* as an approximate low-energy filter by multiplying the initial and final states by M_* for some fixed number of times, L_t',

$$A_{fi}(L_t) = \langle \Psi_f | M_*^{L_t'} M^{L_t} M_*^{L_t'} | \Psi_i \rangle. \tag{30}$$

We use auxiliary fields to generate the interactions contained in our lattice Hamiltonian. The auxiliary field method can be understood as a Gaussian integral formula which relates the exponential of the two-particle density, ρ^2, to the integral of the exponential of the one-particle density, ρ,

$$:\exp\left(-\frac{c\alpha_t}{2}\rho^2\right): = \sqrt{\frac{1}{2\pi}}\int_{-\infty}^{\infty} ds :\exp\left(-\frac{1}{2}s^2 + \sqrt{-c\alpha_t}s\rho\right): . \tag{31}$$

The normal ordering symbol :: ensures that the operator products of the creation and annihilation operators are treated as though classical anticommuting Grassmann variables [10]. We use this integral identity to introduce auxiliary fields defined over every lattice point in space and time [11–13]. As we will see shortly, the pion fields are treated in a manner similar to the auxiliary fields. Each nucleon is independent of the other nucleons and interacts only with the auxiliary and pion fields. If the initial and final states are an antisymmetric tensor product of A single nucleon states, then the projection amplitude for any configuration of auxiliary and pion fields is proportional to the determinant of an $A \times A$ matrix Z_{jk}. The matrix entries of Z_{jk} are single nucleon amplitudes for a nucleon starting at state k and ending at state j.

We couple auxiliary fields s to $\rho_{\rm NL}$ and s_I to $\rho_{I,{\rm NL}}$ for the nonlocal interactions in $V_{\rm NL}$. The terms linear in the auxiliary fields are

$$V_{\rm NL}^{s} = \sqrt{-c_{\rm NL}}\sum_{\mathbf{n}} \rho_{\rm NL}(\mathbf{n}) s(\mathbf{n}) + \sqrt{-c_{I,{\rm NL}}}\sum_{\mathbf{n},I} \rho_{I,{\rm NL}}(\mathbf{n}) s_I(\mathbf{n}), \tag{32}$$

and the terms quadratic field in the auxiliary fields are

$$V_{\rm NL}^{ss} = \frac{1}{2}\sum_{\mathbf{n}} s^2(\mathbf{n}) + \frac{1}{2}\sum_{\mathbf{n},I} s_I^2(\mathbf{n}). \tag{33}$$

We also couple auxiliary fields u to $\rho_{\rm L}$, u_S to $\rho_{S,{\rm L}}$, u_I to $\rho_{I,{\rm L}}$, and $u_{S,I}$ to $\rho_{S,I,{\rm L}}$, for the local interactions in $V_{\rm L}$,

$$\begin{aligned} V_{\rm L}^{u} =& \sqrt{-c_{\rm L}}\sum_{\mathbf{n}} \rho_{\rm L}(\mathbf{n}) u(\mathbf{n}) + \sqrt{-c_{S,{\rm L}}}\sum_{\mathbf{n},S} \rho_{S,{\rm L}}(\mathbf{n}) u_S(\mathbf{n}) \\ &+ \sqrt{-c_{I,{\rm L}}}\sum_{\mathbf{n},I} \rho_{I,{\rm L}}(\mathbf{n}) u_I(\mathbf{n}) + \sqrt{-c_{S,I,{\rm L}}}\sum_{\mathbf{n},S,I} \rho_{S,I,{\rm L}}(\mathbf{n}) u_{S,I}(\mathbf{n}), \end{aligned} \tag{34}$$

$$V_{\rm L}^{uu} = \frac{1}{2}\sum_{\mathbf{n}} u^2(\mathbf{n}) + \frac{1}{2}\sum_{\mathbf{n},S} u_S^2(\mathbf{n}) + \frac{1}{2}\sum_{\mathbf{n},I} u_I^2(\mathbf{n}) + \frac{1}{2}\sum_{\mathbf{n},S,I} u_{S,I}^2(\mathbf{n}). \tag{35}$$

For the one-pion exchange interaction we couple the gradient of the pion field π_I to the point-like density $\rho_{S,I}$,

$$V^{\pi} = \frac{g_A}{2f_\pi}\sum_{\mathbf{n},S,I} \rho_{S,I}(\mathbf{n}') f_S^{\pi}(\mathbf{n}'-\mathbf{n})\pi_I(\mathbf{n}), \tag{36}$$

$$V^{\pi\pi} = \frac{1}{2}\sum_{\mathbf{n},I} \pi_I(\mathbf{n}') f^{\pi\pi}(\mathbf{n}'-\mathbf{n})\pi_I(\mathbf{n}) :, \tag{37}$$

where f_S^{π} and $f^{\pi\pi}$ are defined as

$$f_S^{\pi}(\mathbf{n}'-\mathbf{n}) = \frac{1}{L^3}\sum_{\mathbf{q}} \exp[-i\mathbf{q}\cdot(\mathbf{n}'-\mathbf{n})] q_S, \tag{38}$$

$$f^{\pi\pi}(\mathbf{n}'-\mathbf{n}) = \frac{1}{L^3}\sum_{\mathbf{q}} \exp[-i\mathbf{q}\cdot(\mathbf{n}'-\mathbf{n}) + b_\pi \mathbf{q}^2](\mathbf{q}^2+m_\pi^2). \tag{39}$$

Then the transfer matrices for the LO interactions can be written in following manner. For interaction A we have

$$:\exp\left(-H_A\alpha_t\right): = \int DsD\pi :\exp\left(-H_{\rm free}\alpha_t - V_{\rm NL}^s\sqrt{\alpha_t} - V_{\rm NL}^{ss} - V^\pi\alpha_t - V^{\pi\pi}\alpha_t\right):, \tag{40}$$

where Ds is the path integral measure for s and s_I, and $D\pi$ is the path integral measure for π_I. For interaction B we find

$$\begin{aligned}&:\exp\left(-H_B\alpha_t\right): = \\ &\int DsDuD\pi :\exp\left(-H_{\rm free}\alpha_t - V_{\rm NL}^s\sqrt{\alpha_t} - V_{\rm NL}^{ss} - V_{\rm L}^u\sqrt{\alpha_t} - V_{\rm L}^{uu} - V^\pi\alpha_t - V^{\pi\pi}\alpha_t\right):,\end{aligned} \tag{41}$$

where Du is the path integral measure for u, u_S, u_I, and $u_{S,I}$. See Ref. [10] for details on the Monte Carlo importance sampling algorithms used to calculate the path integrals over the auxiliary and pion fields.

When computing the energy from ratios of amplitudes $A_{fi}(L_t)/A_{fi}(L_t-1)$, previous studies have used importance sampling according to the importance function $|A_{fi}(L_t-1)|$ or $|A_{fi}(L_t)|$. In this work we sample according to a linear combination $x|A_{fi}(L_t-1)| + (1-x)|A_{fi}(L_t)|$ where $0<x<1$. This greatly reduces the stochastic noise because the contributions to $A_{fi}(L_t-1)$ and $A_{fi}(L_t)$ from any individual configuration are now bounded above in magnitude,

$$\frac{|A_{fi}(L_t-1)|}{x|A_{fi}(L_t-1)| + (1-x)|A_{fi}(L_t)|} < x^{-1}, \tag{42}$$

$$\frac{|A_{fi}(L_t)|}{x|A_{fi}(L_t-1)| + (1-x)|A_{fi}(L_t)|} < (1-x)^{-1}. \tag{43}$$

Ground state energies of nuclei

We let $a^\dagger_{\uparrow,p}(\mathbf{n})$, $a^\dagger_{\downarrow,p}(\mathbf{n})$, $a^\dagger_{\uparrow,n}(\mathbf{n})$, and $a^\dagger_{\downarrow,n}(\mathbf{n})$ be the creation operators for a spin-up proton, spin-down proton, spin-up neutron, and spin-down neutron. We write $\tilde{a}^\dagger_{\uparrow,p}(0)$, $\tilde{a}^\dagger_{\downarrow,p}(0)$, $\tilde{a}^\dagger_{\uparrow,n}(0)$, and $\tilde{a}^\dagger_{\downarrow,n}(0)$ for the corresponding zero-momentum creation operators. We also write $\prod\tilde{a}^\dagger$ as shorthand for the product

$$\prod\tilde{a}^\dagger = \tilde{a}^\dagger_{\uparrow,p}(0)\tilde{a}^\dagger_{\downarrow,p}(0),\tilde{a}^\dagger_{\uparrow,n}(0)\tilde{a}^\dagger_{\downarrow,n}(0). \tag{44}$$

For the ground state energy calculations of ^{3}H and ^{3}He we use a lattice volume of (16 fm)^3. The initial states we choose are

$$|\Psi_i^{^3{\rm H}}\rangle = \sum_{\mathbf{n},\mathbf{n}',\mathbf{n}'',\mathbf{n}'''} e^{-\alpha|\mathbf{n}-\mathbf{n}'|}e^{-\alpha|\mathbf{n}-\mathbf{n}''|}e^{-\alpha|\mathbf{n}-\mathbf{n}'''|}a^\dagger_{\uparrow,p}(\mathbf{n}')a^\dagger_{\uparrow,n}(\mathbf{n}'')a^\dagger_{\downarrow,n}(\mathbf{n}''')\,|0\rangle\,, \tag{45}$$

$$|\Psi_i^{^3{\rm He}}\rangle = \sum_{\mathbf{n},\mathbf{n}',\mathbf{n}'',\mathbf{n}'''} e^{-\alpha|\mathbf{n}-\mathbf{n}'|}e^{-\alpha|\mathbf{n}-\mathbf{n}''|}e^{-\alpha|\mathbf{n}-\mathbf{n}'''|}a^\dagger_{\uparrow,n}(\mathbf{n}')a^\dagger_{\uparrow,p}(\mathbf{n}'')a^\dagger_{\downarrow,p}(\mathbf{n}''')\,|0\rangle\,, \tag{46}$$

with $\alpha = 2$ in lattice units. In panel **a** of Fig. S2 we show the energy versus projection time $t = L_t a_t$ for ^{3}He for the LO interaction A (blue plus signs and dashed lines), LO interaction B (red squares and dashed lines), LO + Coulomb interaction A (blue crosses and solid lines), and LO + Coulomb interaction B (red triangles and solid lines). As we are not including isospin-breaking effects other than Coulomb interactions, the LO and LO + Coulomb results for ^{3}H are exactly the same as the LO results for ^{3}He. The error bars indicate one standard deviation errors due to the stochastic noise of the Monte Carlo simulations. The lines are extrapolations to infinite projection time using the ansatz,

$$E(t) = E_0 + c\exp[-\Delta E\, t], \tag{47}$$

where E_0 is the ground state energy that we wish to determine. The results for the ground state energies are shown in Table 1.

FIG. S2: Energy versus projection time for ^{3}H,^{3}He, and ^{4}He. In panels **a** and **b** we plot the energy versus projection time $t = L_t a_t$ for ^{3}He and ^{4}He respectively for the LO interaction A (blue plus signs and dashed lines), LO interaction B (red squares and dashed lines), LO + Coulomb interaction A (blue crosses and solid lines), and LO + Coulomb interaction B (red triangles and solid lines). The LO and LO + Coulomb results ^{3}H are the same as the LO results for ^{3}He. The error bars indicate one standard deviation errors from the stochastic noise of the Monte Carlo simulations, and the lines show extrapolations to infinite projection time.

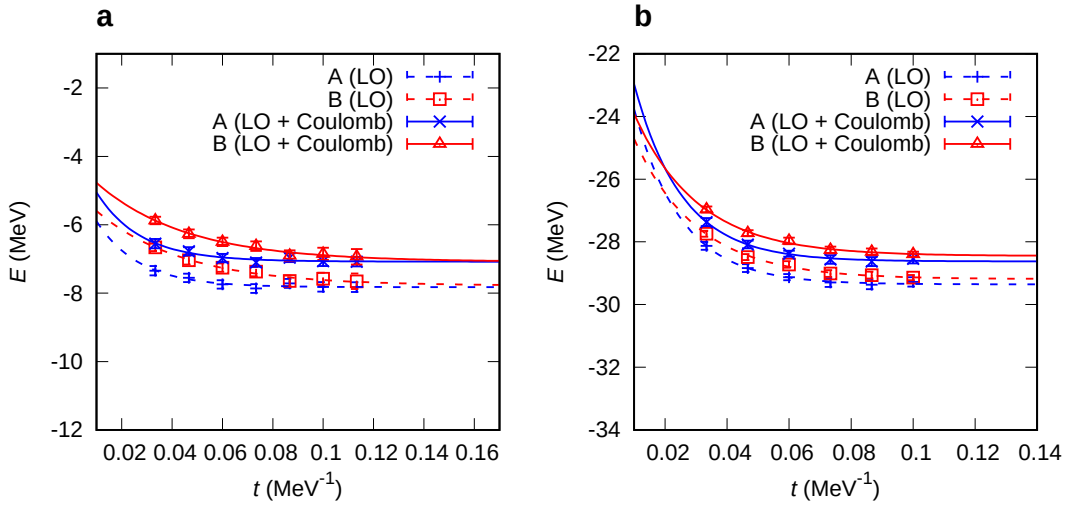

For the ground state energy calculations of ^{4}He we use a lattice volume of $(12\text{ fm})^3$. The initial state we choose is

$$|\Psi_i^{^4\text{He}}\rangle = \prod \tilde{a}^\dagger\,|0\rangle\,. \tag{48}$$

In panel **b** of Fig. S2 we show the energy versus projection time $t = L_t a_t$ for ^{4}He for the LO interaction A (blue plus signs and dashed lines), LO interaction B (red squares and dashed lines), LO + Coulomb interaction A (blue crosses and solid lines), and LO + Coulomb interaction B (red triangles and solid lines). The error bars indicate one standard deviation errors of the Monte Carlo simulations, and the lines are extrapolations to infinite projection time using the ansatz in Eq. (47). The results for the ground state energies are shown in Table 1.

We note that while that the ^{3}H energies for interactions A and B are underbound, the energies for ^{4}He are near the physical value. This may seem puzzling since in continuum-space calculations there is a well-known universal correlation between the ^{3}H and ^{4}He energies called the Tjon line [14–16]. Our lattice results show some deviation from this universal behavior due to lattice artifacts associated with our lattice spacing of 1.97 fm. This is not a new observation. The same behavior has been analyzed previously at the same lattice spacing but with a different lattice interaction [1, 17]. In order to match the physical ^{3}H and ^{4}He energies at the same time, higher-order short-range three-nucleon interactions at N^{4}LO and possibly the leading-order short-range four-nucleon interaction at N^{5}LO are needed. However a much simpler solution is to use a smaller lattice spacing, as these lattice deviations from the continuum-space Tjon line decrease very rapidly with the lattice spacing.

For the ground state energy calculations of ^{8}Be, ^{12}C, ^{16}O, and ^{20}Ne we use a lattice volume of $(12\text{ fm})^3$. The initial states we use are

$$|\Psi_i^{^8\text{Be}}\rangle = \prod \tilde{a}^\dagger \cdot M_* \prod \tilde{a}^\dagger\,|0\rangle\,, \tag{49}$$

$$|\Psi_i^{^{12}\text{C}}\rangle = \prod \tilde{a}^\dagger \cdot M_* \prod \tilde{a}^\dagger \cdot M_* \prod \tilde{a}^\dagger\,|0\rangle\,, \tag{50}$$

$$|\Psi_i^{^{16}\text{O}}\rangle = \prod \tilde{a}^\dagger \cdot M_* \prod \tilde{a}^\dagger \cdot M_* \prod \tilde{a}^\dagger \cdot M_* \prod \tilde{a}^\dagger\,|0\rangle\,, \tag{51}$$

$$|\Psi_i^{^{20}\text{Ne}}\rangle = \prod \tilde{a}^\dagger \cdot M_* \prod \tilde{a}^\dagger \cdot M_* \prod \tilde{a}^\dagger \cdot M_* \prod \tilde{a}^\dagger \cdot M_* \prod \tilde{a}^\dagger\,|0\rangle\,. \tag{52}$$

The interspersing of the transfer matrix M_* in between the products of creation operators allows us to create all nucleons with zero momentum without violating the Pauli exclusion principle. In panels **a, b, c, d** of Fig. S3 we show the energy versus projection time $t = L_t a_t$ for ^{8}Be, ^{12}C, ^{16}O, and ^{20}Ne respectively for the LO interaction A (blue plus signs and dashed lines), LO interaction B (red squares and dashed lines), LO + Coulomb interaction A (blue

crosses and solid lines), and LO + Coulomb interaction B (red triangles and solid lines). The error bars indicate one standard deviation errors from the stochastic noise of the Monte Carlo simulations, and the lines are extrapolations to infinite projection time using the ansatz in Eq. (47). The results for the ground state energies are shown in Table 1.

FIG. S3: Energy versus projection time for ^{8}Be,^{12}C,^{16}O, and ^{20}Ne. In panels **a**, **b**, **c**, **d** we plot the energy versus projection time $t = L_t a_t$ for ^{8}Be, ^{12}C, ^{16}O, and ^{20}Ne respectively for the LO interaction A (blue plus signs and dashed lines), LO interaction B (red squares and dashed lines), LO + Coulomb interaction A (blue crosses and solid lines), and LO + Coulomb interaction B (red triangles and solid lines). The error bars indicate one standard deviation errors from the stochastic noise of the Monte Carlo simulations, and the lines show extrapolations to infinite projection time.

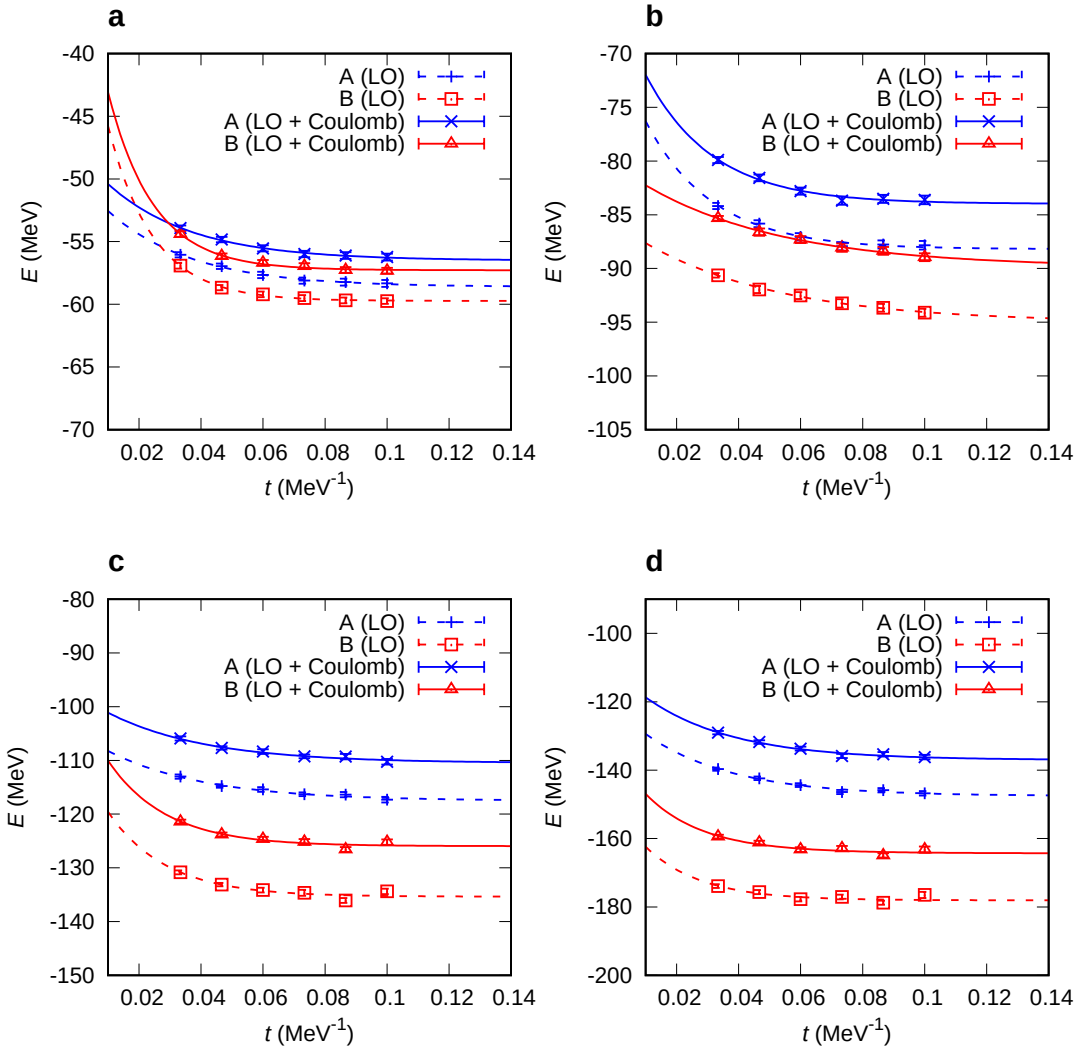

For both interactions A and B, the auxiliary-field Monte Carlo simulations presented here have far milder Monte Carlo sign cancellations than in previous lattice simulations of the same systems [18]. This very promising development will allow for much larger and previously difficult simulations in the future. The savings come from two innovations. The first is the introduction of the nonlocal interactions in $V_{\rm NL}$. Ironically, the implementation of general nonlocal interactions in quantum Monte Carlo simulations have long been problematic due to sign oscillations. However, the auxiliary-field implementation of the interactions in $V_{\rm NL}$ are extremely favorable from the point of view of sign oscillations. The reason for this is the very simple structure of the terms in $V_{\rm NL}$. This leads to fewer issues with so-called interference sign problems as discussed in Ref. [19]. The other innovation reducing the sign problem is the introduction of the parameter b_π in the one-pion exchange interaction. This decreases the short-distance repulsion in the S-wave channels responsible for some sign oscillations.

Adiabatic projection method

The adiabatic projection method is a general framework that produces a low-energy effective theory for clusters of particles which becomes exact in the limit of large projection time. The details of the methods used here were discussed in Ref. [20], and we review some of the main features here. On our L^3 periodic spatial lattice we consider a set of initial two-alpha states $|\mathbf{R}\rangle$ labeled by the spatial separation vector $\mathbf{R}$. For the alpha-alpha scattering calculations presented here we use $L = 16$ fm. The initial alpha wave functions are Gaussian wave packets which, for large $|\mathbf{R}|$, factorize as a product of two individual alpha clusters,

$$|\mathbf{R}\rangle = \sum_{\mathbf{r}} |\mathbf{r} + \mathbf{R}\rangle_1 \otimes |\mathbf{r}\rangle_2. \tag{53}$$

The summation over $\mathbf{r}$ is required to produce states with total momentum equal to zero. As we have done in Eq. (23) for nucleon-nucleon scattering, we project onto spherical harmonics Y_{ℓ,ℓ_z} with angular momentum quantum numbers ℓ, ℓ_z,

$$|R\rangle^{\ell,\ell_z} = \sum_{\mathbf{R}'} Y_{\ell,\ell_z}(\hat{\mathbf{R}}')\delta_{R,|\mathbf{R}'|}|\mathbf{R}'\rangle. \tag{54}$$

We only consider values for $|\mathbf{R}|$ less than $L/2$.

The next step is to multiply by powers of the transfer matrix to form dressed cluster states that approximately span the set of low-energy alpha-alpha scattering states in our periodic box. We start with the approximate transfer matrix M_* as in Eq. (30), and then follow with powers of the leading-order transfer matrix M. After n_t time steps, we have the dressed cluster states

$$|R\rangle_{n_t}^{\ell,\ell_z} = M^{n_t} M_*^{L'_t} |R\rangle^{\ell,\ell_z}. \tag{55}$$

The dressed cluster states are then used to compute matrix elements of the transfer matrix M,

$$[M_{n_t}]_{R',R}^{\ell,\ell_z} = {}_{n_t}^{\ell,\ell_z}\langle R'|M|R\rangle_{n_t}^{\ell,\ell_z}. \tag{56}$$

Since the states are not orthogonal, we compute a norm matrix

$$[N_{n_t}]_{R',R}^{\ell,\ell_z} = {}_{n_t}^{\ell,\ell_z}\langle R'|R\rangle_{n_t}^{\ell,\ell_z}. \tag{57}$$

The radial adiabatic transfer matrix is defined as the matrix product,

$$\left[M_{n_t}^a\right]_{R',R}^{\ell,\ell_z} = \left[N_{n_t}^{-\frac{1}{2}} M_{n_t} N_{n_t}^{-\frac{1}{2}}\right]_{R',R}^{\ell,\ell_z}. \tag{58}$$

Just as we have done for nucleon-nucleon scattering, we impose a spherical hard wall boundary at some radius R_W. For large n_t the standing waves of the radial adiabatic transfer matrix are used to determine the elastic phase shifts for alpha-alpha scattering. As explained in Ref. [20], this scattering calculation is extended out to very large volumes of $L^3 = (120 \text{ fm})^3$ using single alpha-particle simulations and including long-range Coulomb interactions between the otherwise non-interacting alpha particles at large distances.

In Fig. S4 we plot the LO + Coulomb S-wave phase shifts for interaction A at several laboratory energies versus the number of time steps $L_t = 2n_t + 1$. The analogous LO + Coulomb S-wave phase shifts for interaction B are shown in Fig. S5. For both of these figures, the panels **a**, **b**, **c**, **d**, **e**, **f**, **g** correspond to laboratory energies $E_{\text{Lab}} = 1.0$, 2.0, 3.0, 4.5, 6.5, 8.5, 10.0 MeV respectively. The error bars indicate one standard deviation uncertainties due to Monte Carlo errors, and the dot-dashed lines show the extrapolation curve for the $L_t \to \infty$ limit. We use the ansatz

$$\delta_0(L_t, E) = \delta_0(E) + c_0(E)\exp[-\Delta E\, L_t a_t], \tag{59}$$

where $\delta_0(E)$ is the extrapolated phase shift. The hatched regions in Fig. S4 and S5 show the one standard deviation error estimate of the extrapolation.

Tight-binding approximation and potential

The tight-binding approximation is a simple qualitative picture where the alpha particle is treated as a compact object with a small but nonzero radius, R_α. As the name suggests, it is conceptually similar to the tight-binding

FIG. S4: Alpha-alpha S-wave extrapolations for interaction A. LO + Coulomb results (circles) for the S-wave phase shift for interaction A at several laboratory energies versus the number of time steps $L_t = 2n_t + 1$. The panels **a**, **b**, **c**, **d**, **e**, **f**, **g** correspond to laboratory energies $E_{\rm Lab}$ = 1.0, 2.0, 3.0, 4.5, 6.5, 8.5, 10.0 MeV respectively. The error bars indicate one standard deviation uncertainty due to Monte Carlo errors. The dot-dashed lines show the extrapolation to the $L_t \to \infty$ limit, and the hatched regions show the one standard deviation error estimate for the extrapolation.

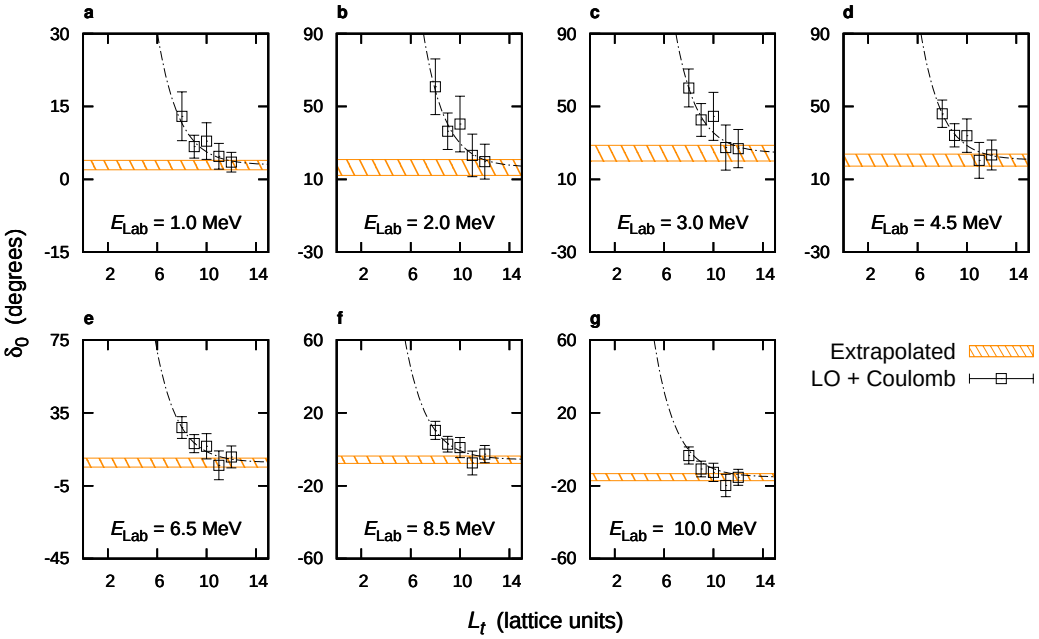

FIG. S5: Alpha-alpha S-wave extrapolations for interaction B. LO + Coulomb results (circles) for the S-wave phase shift for interaction B at several laboratory energies versus the number of time steps $L_t = 2n_t + 1$. The panels **a**, **b**, **c**, **d**, **e**, **f**, **g** correspond to laboratory energies $E_{\rm Lab}$ = 1.0, 2.0, 3.0, 4.5, 6.5, 8.5, 10.0 MeV respectively. The error bars indicate one standard deviation uncertainty due to Monte Carlo errors. The dot-dashed lines show the extrapolation to the $L_t \to \infty$ limit, and the hatched regions show the one standard deviation error estimate for the extrapolation.

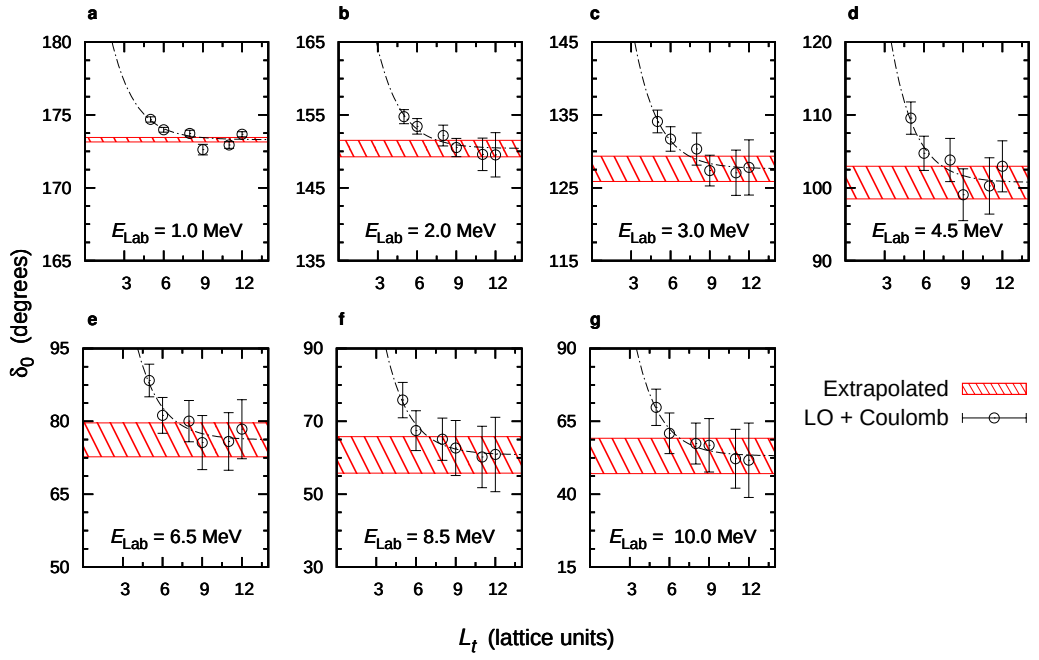

model of electronic structure commonly used in condensed matter physics. Here we provide some further details of the direct and exchange terms in the calculation of the tight-binding potential between two alpha clusters. Let us consider a nucleon-nucleon interaction in continuous space of the form

$$\frac{1}{2}\int d^3\mathbf{R}d^3\mathbf{r}'d^3\mathbf{r}\; V^{s_2,i_2;s_1,i_1}_{s_4,i_4;s_3,i_3}(\mathbf{r}',\mathbf{r})a^\dagger_{s_3,i_3}(\mathbf{R}-\mathbf{r}'/2)a^\dagger_{s_4,i_4}(\mathbf{R}+\mathbf{r}'/2)a_{s_2,i_2}(\mathbf{R}+\mathbf{r}/2)a_{s_1,i_1}(\mathbf{R}-\mathbf{r}/2). \tag{60}$$

The indices s_1, s_2, s_3, s_4 correspond to spin, while i_1, i_2, i_3, i_4 correspond to isospin. For $r > R_\alpha$, the tight-binding potential $V_{\rm TB}(r)$ can be divided into two contributions,

$$V_{\rm TB}(r) = V^{\rm direct}_{\rm TB}(r) + V^{\rm exchange}_{\rm TB}(r), \tag{61}$$

where the direct term is

$$V^{\rm direct}_{\rm TB}(|\mathbf{r}|) = \sum_{s_{24},i_{24}}\sum_{s_{13},i_{13}}\int_{|\mathbf{r}'-\mathbf{r}|<R_\alpha} d^3\mathbf{r}'\; V^{s_{24},i_{24};s_{13},i_{13}}_{s_{24},i_{24};s_{13},i_{13}}(\mathbf{r}',\mathbf{r}), \tag{62}$$

and the exchange term is

$$V^{\rm exchange}_{\rm TB}(|\mathbf{r}|) = -\sum_{s_{23},i_{23}}\sum_{s_{14},i_{14}}\int_{|\mathbf{r}'+\mathbf{r}|<R_\alpha} d^3\mathbf{r}'\; V^{s_{23},i_{23};s_{14},i_{14}}_{s_{14},i_{14};s_{23},i_{23}}(\mathbf{r}',\mathbf{r}). \tag{63}$$

Ground state energies as a function of λ

We consider the one-parameter family of interactions, $V_\lambda = (1-\lambda)V_{\rm A} + \lambda V_{\rm B}$ with the Coulomb interactions switched off. At the phase transition point the alpha clusters become non-interacting in the dilute limit, and so we should find the following simple relationship among the ground state energies provided that the finite volume is sufficiently large:

$$E_{^4{\rm He}} = 1/2\; E_{^8{\rm Be}} = 1/3\; E_{^{12}{\rm C}} = 1/4\; E_{^{16}{\rm O}} = 1/5\; E_{^{20}{\rm Ne}}. \tag{64}$$

In Fig. S6 we plot the LO ground state energies $E_{^4{\rm He}}$, $1/2\; E_{^8{\rm Be}}$, $1/3\; E_{^{12}{\rm C}}$, $1/4\; E_{^{16}{\rm O}}$, $1/5\; E_{^{20}{\rm Ne}}$ versus λ. We see that the phase transition occurs at $\lambda_\infty = 0.0(1)$.

FIG. S6: Ground state energies versus λ. We plot the LO ground state energies $E_{^4{\rm He}}$, $1/2\; E_{^8{\rm Be}}$, $1/3\; E_{^{12}{\rm C}}$, $1/4\; E_{^{16}{\rm O}}$, $1/5\; E_{^{20}{\rm Ne}}$ versus the parameter λ which interpolates between $V_{\rm A}$ and $V_{\rm B}$.

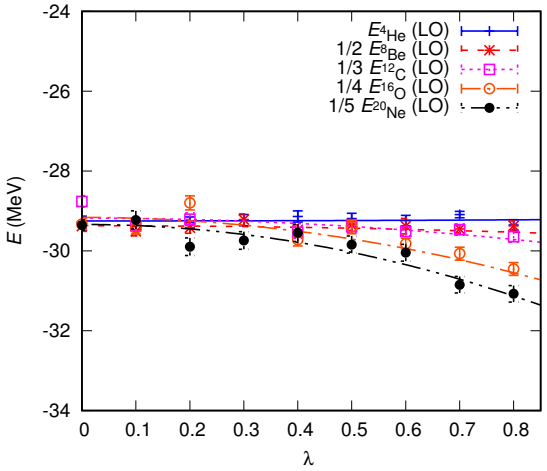

To determine the critical point λ_{20} when ^{20}Ne becomes bound, we compare $E_{^{20}{\rm Ne}}$ with the threshold energy $E_{^{16}{\rm O}}$ + $E_{^4{\rm He}}$. For this analysis we also include the finite-volume energy one obtains at infinite S-wave scattering length for the ^{16}O + ^{4}He system. At infinite scattering length the energy of any two-body system with reduced mass μ in a periodic box of size L is [21, 22]

$$\Delta E = \frac{4\pi^2 d_1}{mL^2}, \tag{65}$$

where

$$d_1 \approx -0.095901. \tag{66}$$

We find that the critical point for the binding of ^{20}Ne is $\lambda_{20} = 0.2(1)$. A similar analysis for the binding of the other alpha nuclei finds $\lambda_{16} = 0.2(1)$ for ^{16}O, $\lambda_{12} = 0.3(1)$ for ^{12}C, and $\lambda_8 = 0.7(1)$ for ^{8}Be.

Code Availability

All codes used in this work are freely available and can be obtained by contacting the authors.

[1] E. Epelbaum, H. Krebs, D. Lee, and U.-G. Meißner, Eur. Phys. J. **A45**, 335 (2010), arXiv:1003.5697 [nucl-th].
[2] N. Klein, D. Lee, W. Liu, and U.-G. Meißner, Phys. Lett. **B747**, 511 (2015), 1505.07000.
[3] J. Carlson, V. Pandharipande, and R. Wiringa, Nucl. Phys. A **424**, 47 (1984), ISSN 0375-9474, URL http://www.sciencedirect.com/science/article/pii/0375947484901271.
[4] B. Borasoy, E. Epelbaum, H. Krebs, D. Lee, and U.-G. Meißner, Eur. Phys. J. **A34**, 185 (2007), arXiv:0708.1780 [nucl-th].
[5] B.-N. Lu, T. A. Lähde, D. Lee, and U.-G. Meißner (2015), 1506.05652.
[6] V. G. J. Stoks, R. A. M. Kompl, M. C. M. Rentmeester, and J. J. de Swart, Phys. Rev. **C48**, 792 (1993).
[7] E. Wigner, Phys. Rev. **51**, 106 (1937).
[8] J.-W. Chen, D. Lee, and T. Schäfer, Phys. Rev. Lett. **93**, 242302 (2004), nucl-th/0408043.
[9] D. Lee, Phys. Rev. Lett. **98**, 182501 (2007), nucl-th/0701041.
[10] D. Lee, Prog. Part. Nucl. Phys. **63**, 117 (2009), arXiv:0804.3501 [nucl-th].
[11] J. Hubbard, Phys. Rev. Lett. **3**, 77 (1959).
[12] R. L. Stratonovich, Soviet Phys. Doklady **2**, 416 (1958).
[13] S. E. Koonin, Journal of Statistical Physics **43**, 985 (1986), ISSN 0022-4715, URL http://dx.doi.org/10.1007/BF02628325.
[14] J. Tjon, Physics Letters B **56**, 217 (1975), ISSN 0370-2693, URL http://www.sciencedirect.com/science/article/pii/0370269375903780.
[15] A. Nogga, H. Kamada, and W. Gloeckle, Phys. Rev. Lett. **85**, 944 (2000), nucl-th/0004023.
[16] L. Platter, H.-W. Hammer, and U.-G. Meißner, Phys. Lett. **B607**, 254 (2005), nucl-th/0409040.
[17] E. Epelbaum, H. Krebs, D. Lee, and U.-G. Meißner, Phys. Rev. Lett. **104**, 142501 (2010), arXiv:0912.4195 [nucl-th].
[18] T. A. Lähde, E. Epelbaum, H. Krebs, D. Lee, U.-G. Meißner, and G. Rupak, Phys. Lett. **B732**, 110 (2014), 1311.0477.
[19] T. A. Lähde, T. Luu, D. Lee, U.-G. Meißner, E. Epelbaum, H. Krebs, and G. Rupak, Eur. Phys. J. **A51**, 92 (2015), 1502.06787.
[20] S. Elhatisari, D. Lee, G. Rupak, E. Epelbaum, H. Krebs, T. A. Lähde, T. Luu, and U.-G. Meißner, Nature **528**, 111 (2015), 1506.03513.
[21] D. Lee, Phys. Rev. **B73**, 115112 (2006), cond-mat/0511332.
[22] S. R. Beane, P. F. Bedaque, A. Parreno, and M. J. Savage, Phys. Lett. **B585**, 106 (2004), hep-lat/0312004.